morphological and ferroelectric studies of Li-doped ZnO thin films

Veronique Bornand, Mezy Aude

Morphological and ferroelectric studies of Li-doped ZnO thin films

V. Bornand, A. Mezy

Institut Charles Gerhardt, ICGM UMR CNRS 5253, UM2, Place E. Bataillon, CC1504, F-34095 Montpellier cedex 5, France

Abstract

Li-doped ZnO films were grown on glass substrates by ultrasonic spray pyrolysis (pyrosol) and chemical bath deposition (CBD) methods. A comparative study was performed on the effect of Li doping (0-40at%) on the morphology and ferroelectric properties of such as-grown films. Structural investigations revealed that, in both cases, high-quality layers were grown with the wurtzite structure and *c*-axis preferred crystalline orientation. The surface morphology and grain structure depended on the deposition process as well as the physical properties induced by Li-doping. The temperature during the initial stage of the growth appeared as an important parameter. Ferroelectricity in Li-doped ZnO films could be observed only for the lower-temperature CBD process in which diffusion phenomena at the film/substrate interface were limited.

Keywords

Doped zinc oxide, Li-doped ZnO; pyrosol, chemical bath deposition, thin films, ferroelectrics

Introduction

ZnO is extensively studied as a prospective material for electronic and optoelectronic devices where high quality ZnO films are required. Several methods have been developed for controlling the geometry, thickness and morphology of these films and related properties, including r.f. sputtering [1], pulsed laser deposition [2], chemical vapor deposition [3], sol-gel [4], ultrasonic spray pyrolysis [5], chemical bath deposition [6]. In our recent works, we presented an alternative approach for the oriented growth of ZnO nanostructures by ultrasonic spray pyrolysis (pyrosol) assisted chemical bath deposition (CBD) process [7].

Paralleling the world-wide interest in pure ZnO, there is also a rapidly growing research effort aimed at exploring doped-ZnO nanostructures. Ferromagnetism could be observed in ZnO:Mn, ZnO:Cu, ZnO:Fe thin films while ferroelectricity could be induced in ZnO:Li materials, although the origin of these properties is currently controversial [8-11]. Different

theories of the origin of ferromagnetic/ferroelectric ordering were proposed, including theories based on intrinsic defect involvement as well as free carrier mediated mechanisms.
In this work, Li-doped (0-40at%) thin films were grown on glass substrates by ultrasonic spray pyrolysis (pyrosol) and chemical bath deposition (CBD) methods. These two low-temperature deposition processes have proved to be simple and inexpensive, requiring minor laboratorial efforts. One aim of the present study was to examine their potential and effectiveness in the growth of ZnO:Li films offering new functionalities for future ZnO-based devices. A comparative study of the two techniques was performed, focusing on the impact of a Li-doping on the morphological and physical properties of such as-grown materials.

Material and Methods

$Zn_{1-x}Li_xO_y$ films (x = 0.1, 0.2, 0.4) were deposited on glass substrates by pyrosol and CBD in an air atmosphere. More details of the experimental sets up can be found elsewhere [6; 12]. In pyrosol experiments, the initial solutions were prepared from Zinc acetylacetonate [0.01M] and Lithium acetylacetonate dissolved in ethanol and dispersed using an ultrasonic nebulizer. All films were deposited at 450°C during 4h with a flow rate of the solution fixed at 80ml/h. The main advantage of the pyrosol process is a self-induced crystallized growth during the deposition. No subsequent treatments were applied. Growths by CBD proceeded in two steps, starting with a seeding step followed by a final crystallization growth. During the first step, the glass slides were immersed for 20 seconds in Zinc acetate dihydrate [0.2M] isopropanolic solutions held at room temperature in which diethanolamine (DEA) was used as complexing reagent and distilled water as polymerization activator. This procedure was repeated five times, followed by a subsequent annealing at 550°C during 1h30. The second step consisted in the growth of Li-doped ZnO layers on these seeded substrates during 2h. The solutions for CBD were prepared from Zinc nitrate [0.025M] and Hexamethylentetramine (HMTA) [0.025M] dissolved in distilled water in which Lithium nitrate was added. The dip coatings were performed at 90°C, followed by a final annealing at 550°C during 1h30.
The structure and the crystallographic orientation were determined by X-ray diffraction using a X'PERT diffractometer in a full angular range. The surface morphology and film cross-section images were obtained by Scanning Electron Microscopy (SEM) and Atomic Force Microscopy (AFM). Ferroelectric experiments were performed with a RT66A tester.

Results and discussion

The structural properties of undoped and Li-doped ZnO nanostructures produced by pyrosol and CBD were investigated by XRD (Fig 1). All samples showed the hexagonal monophasic ZnO structure (ZnO powder wurtzite) and possessed a (002) texture due to its lowest surface free energy and fastest growth direction [13]. There were no diffraction peaks detected for Li oxide secondary phases or other impurity phases within the sensitivity of our XRD measurements, implying that Li ions were incorporated into the ZnO lattice by substituting on Zn lattice sites. In pyrosol experiments, better crystalline quality and improved *c*-preferential oriented growth could be achieved by increasing Li content. In such a deposition method via vapor phases, nucleation and growth steps occur simultaneously, thus resulting in a limited density of germs at the surface of the substrate and a self-limitation of the out-of plane texturation. Indeed, the number of nuclei formed at the beginning of the growth is predominant in the final orientation of the structures. The improvement of the film alignment with Li could be correlated with the increase of the surface mobility of the Li-based adatoms – lighter and smaller than Zn-based adatoms – concomitant with an increase of the number of nuclei. On contrary, no changes were observed whatever the composition in two-steps growth CBD derived samples. The first seeding step stabilized the whole growth process. In both cases, *c*/*a* ratio and overall deformation remained constant within the tested Li range.

Figures 2 and 3 show the planar AFM images and cross-sectional SEM images of Li(40at%)-doped ZnO samples. In both cases, nanotips with well-defined hexagonal shapes could be observed on top of the nanowires (inset in Fig. 2b), in good accordance with the *c*-oriented growth observed by XRD. In the case of one-step syntheses by pyrosol, lateral growth is more dominant than axial growth at the early growth stage, resulting in largest crystallites. To minimize the film/substrate interface and, thus, reduce the interfacial energy, the crystallites grew with a reversed-pyramid shape (Fig. 3a). However, increasing the Li doping led to finer morphologies compared to undoped ZnO materials [7]. The great advantage of CBD is the sequential growth process, with separated nucleation and growth stages, which enables the deposition of highly oriented layers with well-defined and dense features as well as uniform granulation arrangement (Fig. 3b). Because of the high density of germs formed during the seeding step, the atoms nucleated and formed islands close-packed enough to (1) prevent their in-plane spread during the coalescence step and (2) develop nanorods with regular size and shape, almost perpendicular to the substrate. Contrary to pyrosol-deposited samples, no essential change in the morphology of the microrods was observed in CBD-deposited materials with the increase of Li doping.

Ferroelectric polarization versus electric field (P_r-E) curves of Li(40at%)-doped ZnO samples are presented in Figure 4. Higher voltages were not applied to avoid sample damage. No significant response could be obtained in pyrosol-generated samples. On contrary, layers deposited by CBD showed a hysteresis loop which confirmed the existence of ferroelectricity in these Li-doped ZnO nanostructures. Due to the large surface to volume ratio in 1*D*-ZnO nanostructures, it is expected that the surface states and the diversity in defect concentration and nature play a crucial role in the ferroelectric properties of doped ZnO materials. In pyrosol experiments, the first stage consists in the production of (Zn, Li) vapor and its transport towards the heated substrates. The second stage is the impingement of the species on the substrate surface, their condensation and their nucleation. The final and simultaneous growth stage of the process involves interactions with the substrate, including reevaporation, possible diffusion at the interface and crystal growth itself. Interfacial or superficial phenomena as well as diffusion mechanisms between grain boundaries can be induced by the temperature (450°C) and can explain the absence of hysteresis loops for this method of synthesis. Better results are obtained by CBD. The first seeding layer is close-packed enough to decrease the level of defects at the grain boundaries and minimize diffusion mechanisms and conductive effects during the second independent growth step at rather low temperature (90°C). The origin of this ferroelectric behavior could be explained on the basis of the ionic radius difference between Zn^{2+} (0.74Å) and Li^{+} (0.6Å). Due to this ionic size difference, Li^{+} can occupy off-centered positions. This leads to permanent local electric dipoles and thereby induces ferroelectric behavior [14]. Another origin of ferroelectricity may be due to the existence of oxygen vacancies. Recent investigations have confirmed the role of oxygen vacancies in determining the degree of coupling between the dipoles and in forming long-range and short-range ordering [15]. Similar results have been reported for the appearance of ferroelectricity in Li-doped ZnO films [16,17]. However the relatively high value of remanent polarization (P_r = 2.75 μm/cm^2) we obtained in Li(40at%)-ZnO doped samples compared to bulk Li-ZnO found in the literature (P_r = 2.32 μm/cm^2) highlights its potential reliability in nanoscale nonvolatile ferroelectric memory devices [18].

Conclusions

In this manuscript, we studied the structural and ferroelectric properties of Li-doped ZnO layers deposited by pyrosol and CBD processes. It was found that the films were polycrystalline, with a wurzite (hexagonal) structure. The film crystallites were oriented with the (002) plane parallel to the substrate. This degree of out-of-plane texturation along the *c*-

axis is independent of the Li ratio for CBD-deposited materials but it increased with Li doping in the case of pyrosol-deposited films. The polycrystalline structure of the films and their morphological characteristics played an important role in the mechanisms of ferroelectricity induced by Li doping. The absence of ferroelectric capabilities in pyrosol-deposited materials could be related to an increase of defects levels at the boundaries (such as charge carriers…) compared to CBD-synthesized nanostructures.

References

[1] Hsu YS, Lin J, Tang WC. J Mater Sci Mater Electron 2008; 19:653-61.

[2] Dong W, Zhu X, Tao R. J Mater Sci Mater Electron 2008; 29:538-42.

[3] Kwak CH, Kim BH, Park SH, Seo SY, Park Cl, Kim SH et al. J Cryt Growth 2009; 311:4491-4.

[4] Zhang CY, Li XM, Zhang X, Yu WD, Zhao JL. J Cryst Growth 2006; 290:67-72.

[5] Htay M, Hashimoto Y, Momose N, Ito K. J Cryst Growth 2009; 311:4499-504.

[6] Mezy A, Gerardin C, Tichit D, Suwanboon S, Ravot D, Tedenac JC et al. Mater Res Soc Symp Proc 2006; 601:Rb15-05: 1-6.

[7] Bornand V, Mezy A. Mat Let 2011; 65:1363-66.

[8] Yilmaz S, Bacaksiz E, McGlynn E, Polat I, Ozcan S. Thin Solid Films 2012; 520:5172-58.

[9] Zou CW, Wang HJ, Yin ML, Li M, Liu CS, Guo LP, Fu DJ, Kang TW. J Crsyt Growth 2010; 312:906-9.

[10] Soumahoro I, Moubah R, Schmerber G, Colis S, Ait Aouaj M, Adb-lefdil M, Hassanain. Thin Solid Films 2010; 518:4593-96.

[11] Wang XS, Wu ZC, Webb JF, Liu ZG. Appl Phys A 2003; 77:561-5.

[12] Bornand V, Huet I, Papet P. Mat Chem Phys 2002; 77: 571-7.

[13] Wang ZL, kong XY, Ding Y, Gao P, Hughes WL, Yang R, Zhang Y. Adv Funct Mat 2004; 14:943-56.

[14] Onodera A, Tamaki N, Jin K, Yamashita H. Jon J Appl Phys 1997; 36:6008

[15] Onodera A, Tamaki N, Yamashita H. Jpn J Appl Phys 1996; 35:5160-62.

[16] Zou CW, Shao LX, Guo LP, Fu DJ, Kong TW. J Cryst Growth 2011; 331:44-8.

[17] Gupta MK, Kumar B. J Alloys Comp 2011; 509:L208-12.

[18] Wu ZC, Zhang XM, Liu JM, Li QC, Chen XY, Yin J, Xu N, Liu ZG. Ferroelectrics 2001; 252:265-71.

Figure 1. X-ray diffraction pattern of Li-doped ZnO films deposited on glass substrates by (a) pyrosol and (b) CBD.

Figure 2. AFM images of the surface of Li-doped ZnO films (Li: 40at%) grown by (a) pyrosol and (b) CBD on glass substrate (investigations on 5μm*5μm area).

Figure 3. SEM images of the cross-section of Li-doped ZnO films (Li: 40at%) grown by (a) pyrosol and (b) CBD on glass substrate.

Figure 4. Room temperature (P_r-E) curves of Li-doped ZnO films (Li: 40at%) grown by pyrosol and CBD on glass substrate.

(a)

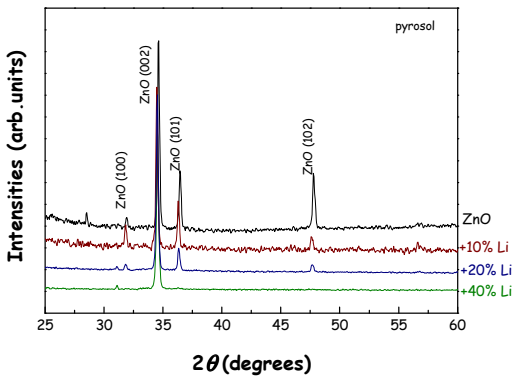
pyrosol
ZnO (002)
ZnO (101)
ZnO (100)
ZnO (102)
Intensities (arb.units)
ZnO
+10% Li
+20% Li
+40% Li
25
30
35
40
45
50
55
60
2θ (degrees)

(b)

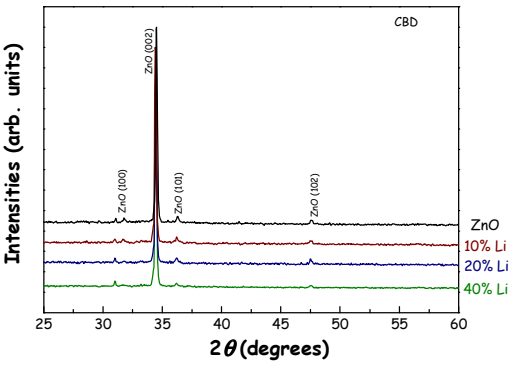
CBD
ZnO (002)
ZnO (100)
ZnO (101)
ZnO (102)
Intensities (arb. units)
ZnO
10% Li
20% Li
40% Li
25
30
35
40
45
50
55
60
2θ (degrees)

Figure 1.

(a)

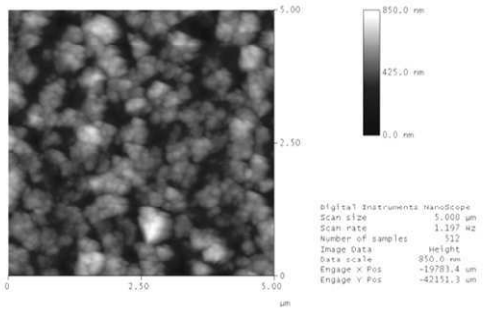
5.00
2.50
0
0
2.50
5.00
µm
850.0 nm
425.0 nm
0.0 nm
Digital Instruments NanoScope
Scan size 5.000 µm
Scan rate 1.197 Hz
Number of samples 512
Image Data Height
Data scale 850.0 nm
Engage X Pos -19783.4 um
Engage Y Pos -42151.3 um

(b)

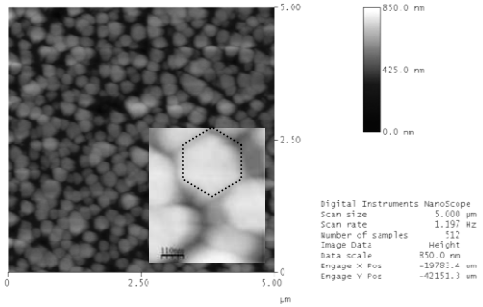
5.00
2.50
0
0
2.50
5.00
µm
850.0 nm
425.0 nm
0.0 nm
Digital Instruments NanoScope
Scan size 5.000 µm
Scan rate 1.197 Hz
Number of samples 512
Image Data Height
Data scale 850.0 nm
Engage X Pos -19783.4 um
Engage Y Pos -42151.3 um

Figure 2

(a)

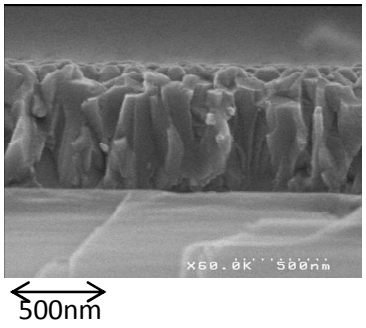

500nm

(b)

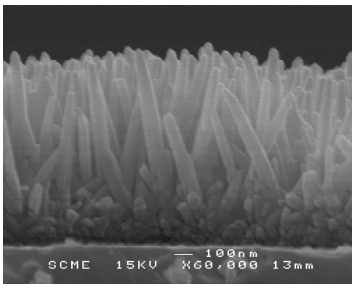

500nm

Figure 3

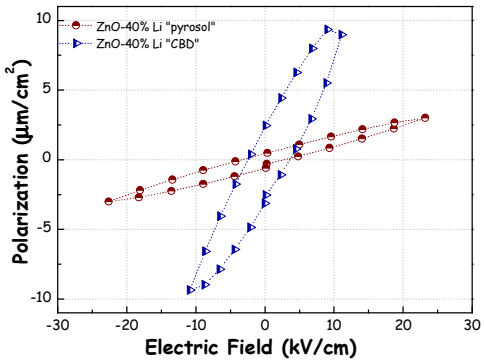
ZnO-40% Li "pyrosol"
ZnO-40% Li "CBD"
Polarization (µm/cm²)
Electric Field (kV/cm)
10
5
0
-5
-10
-30
-20
-10
0
10
20
30

Figure 4.